ORIGINAL ARTICLE

A Comparison of Wavelet Packet, Wavelet Leaders Multifractal, and *p*-Leader Multifractal Method in Chatter Detection

Zehui Zheng[1] · Xiubing Jing[1] · Yangyang Wang[1] · Xiaofei Song[2] · Huaizhong Li[3]

Abstract

An efficient stability analysis contributes to the improvement of machining stability and chatter suppression. First, this paper presents three chatter detection approaches that were developed on the application of wavelet transforms. Second, the feasibility of the methods for chatter detection is verified by combining numerical simulations and experimental research. Finally, the recognition performance of the three methods is compared. The analysis results indicate that the proposed three methods can distinguish different machining states. The *p*-leader multifractal method (PLMM) provides the best recognition performance but takes the longest time, the wavelet leader multifractal method (WLMM) comes second, and the wavelet packet method (WPM) is the worst but takes the shortest amount of time. Therefore, the PLMM can be used for identifying signals with high accuracy requirements, whereas the WLMM or WPM can be used otherwise.

Highlights

- Three methods for judging the stability of micro milling process are proposed by using wavelet packet method (WPM), wavelet leaders multifractal method (WLMM) and p-leader multifractal method (PLMM).

- The feasibility of WPD, WLMM, and PLMM in stability analysis was preliminarily verified through numerical simulation.

- The recognition performance of WPD, WLMM, and PLMM for chatter detection is compared.

✉ Xiubing Jing
jingxiuping@tju.edu.cn

✉ Xiaofei Song
xiaofeisong@tju.edu.cn

1 School of Mechanical Engineering, Tianjin University, Tianjin 300354, China

2 Key Laboratory of Advanced Ceramics and Machining Technology of Ministry of Education, Tianjin University, Tianjin 300354, China

3 Griffith School of Engineering, Gold Coast Campus, Griffith University, Brisbane, QLD 4222, Australia

1 Introduction

Chatter is a self-excited vibration of a tool–workpiece system that often occurs in high-speed milling. It is the main cause of instability in the machining process. The chatter frequency is close to the natural frequency of a machine system when chatter happens [1]. Chatter not only restricts machining precision and efficiency but also causes tool wear and even breakage [2]. Thus, chatter detection methods are of great importance for solving the chatter problem and greatly contribute to the development of intelligent machine tools and manufacturing techniques [3].

Scholars have proposed many chatter detection methods in the past decades, which are mainly divided into three types, i.e., time-domain (TD) analysis, frequency-domain (FD) analysis, time–frequency-domain analysis [4]. It is difficult to highlight the signal characteristics of transient

sudden changes due to the TD and FD analysis focusing on the whole signal. The time–FD analysis provides a good solution to this problem, in which the wavelet transform (WT) is widely utilized. The WT is developed based on the fast Fourier transform and has a good partial characterization performance [5]. The wavelet packet transform develops and extends the WT to refine and reconstruct signals, which has been applied for extracting signal features. With a weighting of the energy for the frequency band containing chatter information, Sun [6] presented a real-time chatter monitoring approach based on the weighted wavelet packet entropy, which is highly sensitive to energy variations caused by chattering. Zhang et al. [7] proposed a chatter recognition approach during milling based on the energy entropy of variational mode decomposition and wavelet packet decomposition (WPD). Based on the relative wavelet packet energy entropy, Yao et al. [8] proposed a real-time monitoring method for tool chatter on computer numerical control (CNC) machines. Hao et al. [9] proposed a novel chatter detection methodology based on WPD and energy entropy for multi-source signal fusion, which can effectively identify early chatter and different levels of chatter.

The fractional analysis method has been gradually developed and applied based on WTs. Ji et al. [10] applied a single-fractal analysis for chatter detection. The multifractal analysis method can fully show the singularity distribution of signals and describe local-scale behaviors more accurately compared with a single-fractal analysis. Wavelet transform modulus maxima (WTMM) and multifractal detrended fluctuation analysis (MF-DFA) are two typical multifractal methods that are often used in bearing fault diagnosis. Wang et al. [11] proposed a chatter detection method based on WTMM. Liu [12] suggested a bearing fault diagnosis approach based on MF-DFA.

Lashermes et al. [13] proposed a new multifractal analysis method based on wavelet leaders, which has solid theoretical mathematical support and avoids complex calculations. This new method provides a powerful way to extract multifractal features, which has been successfully applied for the fault diagnosis of rotating mechanisms [14], heart rate variability (HRV) [15], and structural damage detection [16].

Leonarduzzi et al. [17] introduced an additional parameter p based on wavelet leaders and proposed a p-leader multifractal method to significantly improve the performance of the multifractal spectrum evaluation. Currently, the method is used for HRV classification [18], acidosis detection [19], and chatter detection [20]. All the methods described above are based on the WT, of which WTMM, MF-DFA, wavelet leader multifractal method (WLMM), and p-leader multifractal method (PLMM) belong to the multifractal analysis category, whereas the others

(including the wavelet packet method (WPM)) fall under the WPD category.

Despite the considerable research efforts by scholars in chatter recognition, there is still a great gap in comparing the evaluation performance of chatter detection methods, which limits their industrial application to some extent. In this study, we analyze the feasibility of using the WPM, WLMM, and PLMM in chatter detection and compare their recognition performance. This study will also lay a fundamental reference for the selection of chatter detection methods in the future. The rest of this paper is organized as follows: Sect. 2 describes the basic theory of the WPM, WLMM, and PLMM; Sect. 3 presents the numerical simulation, feasibility, and comparison of the WPM, WLMM, and PLMM for chatter detection; and Sect. 4 outlines some conclusions.

2 Description of the WPM, WLMM, and PLMM

2.1 Description of the WPM

2.1.1 WPD

In this paper, X is used to represent signals. X with length L can be decomposed at m-level to obtain 2^m sets of sub-signals with length $L/2^m$, and the decomposed sub-signals respond to different frequency bands from low to high. Let f_s be the sampling frequency of signal X, then the frequency band of the ith sub-signal can be expressed as $[(i-1)f_s/2^m, if_s/2^m]$, where $i = 1, 2, 3, \ldots, 2^m$. The signal X can be filtered by high-pass and low-pass filters to obtain two sub-signals (D_j and A_j) [21]:

$$D_j[i] = \sum_{k=0}^{\infty} X[k] \cdot h[2i - k], \tag{1}$$

$$A_j[i] = \sum_{k=0}^{\infty} X[k] \cdot l[2i - k], \tag{2}$$

where j is the level of WPD, and h and l represent the high-pass and low-barrel filters, respectively.

2.1.2 WPD Energy Entropy

The WPD energy entropy can be applied to describe the characteristic of a signal. Applying WPD on X can derive a series of sub-signals ($x_1(t), x_2(t), x_3(t), \ldots, x_n(t)$). The energy of each sub-signal (E_i) can be obtained by

$$E_i = \int_{-\infty}^{\infty} x_i^2(t)\mathrm{d}t \quad (i = 1, 2, 3, \ldots, n) \tag{3}$$

According to Eq. (3), the total energy E ($E = \sum_{i=1}^{n} E_i$), energy ratio η_i ($\eta_i = \frac{E_i}{E}$), and energy entropy P ($P = \sum_{i=1}^{n} [-\eta_i \ln(\eta_i)]$) of the signal can be calculated. The energy entropy becomes larger with a uniform energy distribution and smaller with a concentrated energy distribution [22]. Therefore, the energy concentrates at a chatter frequency when chatter occurs, and presumably, the signal will have a small entropy value at this time.

2.2 Description of WLMM

2.2.1 Definition of Wavelet Leaders

Selected $\psi_0(t)$ as the mother wavelet with a compact time support, the positive integer N_ψ is a vanishing moment [23] $\psi_0(t)$ and N_ψ satisfies the following requirements:

$$\int_R t^k \psi_0(t)\mathrm{d}t \equiv 0 \int_R t^{N_\psi} \psi_0(t)\mathrm{d}t \neq 0 \quad (\forall k = 0, 1, \ldots, N_\psi - 1) \tag{4}$$

$\{\psi_{j,k}(t) = 2^{-j/2}\psi_0(2^{-j}t - k), j, k \in Z\}$ is used to represent the templates of $\psi_0(t)$ dilated to scales 2^j and translated to time positions $2^j k$. Accordingly, they form an orthonormal basis of $L^2(R)$.

Discrete wavelet transform is performed on signal X ($X = \{x_k, k \in Z\}$), and the transform coefficient is as follows:

$$c_{j,k} = \int_R X(t)2^{-j}\psi_0(2^{-j}t - k)\mathrm{d}t \tag{5}$$

The binary interval is defined as $\lambda = \lambda_{j,k} = [k \cdot 2^j, (k + 1) \cdot 2^j]$. Let 3λ represent the union of the interval λ with its two adjacent merge element intervals: $3\lambda_{j,k} = \lambda_{j,k-1} \cup \lambda_{j,k} \cup \lambda_{j,k+1}$. The wavelet leaders are defined as the local highest values of the wavelet coefficients in the 3 neighborhood, taking values at all finer scales [13, 24]:

$$L_X(j,k) \equiv L_\lambda = \sup_{\lambda' \subset 3\lambda} |c_{X,\lambda'}| \tag{6}$$

2.2.2 Multifractal Formalism of Wavelet Leaders

Let $S_L(q,j)$ denote the wavelet leader-based structure functions and the corresponding scaling exponents are expressed as $\zeta(q)$, where q represents the order magnitude of the multiresolution quantities [25]:

$$S_L(q,j) = \frac{1}{n_j} \sum_{k=1}^{n_j} |L_X(j,k)|^q \tag{7}$$

$$\zeta_L(q) = \liminf_{j \to 0} \left(\frac{\log_2(S_L(q,j))}{j} \right) \tag{8}$$

The multifractal spectrum ($D(h)$) can be obtained by performing the Legendre transformation on the scaling exponents:

$$D(h) = \inf_{q \neq 0}(1 + qh - \zeta_L(q)) \tag{9}$$

2.3 Description of PLMM

2.3.1 Definition of the *p*-leader

According to Eqs. (4–6), p-leaders corresponding to the signal X are denoted as $l_X^{(p)}(j,k)$ and used to evaluate 3λ [26].

$$l^{(p)}(j,k) \equiv l_\lambda^{(p)} = \left(\sum_{j' \leq j, \lambda' \subset 3\lambda} \sum_{i=1}^{2^d-1} \left| c_\lambda^{(i)} \right|^p 2^{-d(j-j')} \right)^{1/p} \tag{10}$$

Let $p > 0$, and when $p = \inf$, p-leaders become the classical wavelet leaders [26]:

$$l^{\inf}(j,k) \equiv l_\lambda = \sup_{i \in [1,\ldots,2^d-1], j' \leq j, \lambda' \subset 3\lambda} |c_{\lambda'}| \tag{11}$$

2.3.2 Multifractal Formalism of the *p*-leader

The p-leader multifractal spectrum of signal X is defined as follows:

The pointwise p-exponent $h_p(x_0)$ at x_0 on signal X can be expressed as [27, 28]

$$h_p(x_0) = \liminf_{j \to -\infty} \frac{\log(l_{\lambda_{j,k(x_0)}}^{(p)})}{\log(2^j)} \tag{12}$$

The multifractal p-spectrum $D^{(p)}(h)$ can be expressed as

$$D^{(p)}(h) = \dim_H(\{x \in R^d, h_p(x) = h\}) \tag{13}$$

Equation (13) shows that the value h of the Hausdorff dimension $\dim_H$ at x_0 determines the p-leader multifractal spectrum ($D^{(p)}(h)$).

$S_L^{(p)}(j,q)$ and $\zeta^{(p)}(q)$ represent the structure function of p-leaders and the scaling function, respectively [17].

$$S_L^{(p)}(j,q) = 2^{dj} \sum_k (l_{j,k}^{(p)})q \quad (\forall q \in R) \tag{14}$$

$$\zeta^{(p)}(q) = \liminf_{j \to -\infty} \frac{\log(S_L^{(p)}(j,q))}{\log(2^j)} \quad (\forall q \in R) \tag{15}$$

The Legendre transformation can be performed for the mapping $q \to \zeta^p(q)$ to obtain a multifractal formalism of the corresponding signal.

$$L^{(p)}(h) = \inf_{q \in R}(d + qh - \zeta^{(p)}(q)) \tag{16}$$

When $\eta_x(p) > 0$, $\forall h$, $D^{(p)}(h) \le L^{(p)}(h)$. $\eta_x(p)$ is the wavelet scale function, which satisfies the following relation:

$$\eta_x(p) = \liminf_{j \to -\infty} \frac{\log(S_c(j,q))}{\log(2^j)} \quad (\forall p > 0) \tag{17}$$

It provides practitioners with an upper bound for $D^{(p)}(h)$:

$$D^{(p)}(h) \le L^{(p)}(h) = \inf_{q \in R}(d + qh - \zeta^{(p)}(q)) \tag{18}$$

3 Results and Discussion

3.1 Numerical Simulation Analysis

The vibration signals are simulated as follows [29, 30]:

$$X_{\text{Stable}} = 2\sin(30\pi t) + 2.5\sin(60\pi t) + 3\sin(90\pi t) \tag{19}$$

$$\begin{aligned} X_{\text{Weak−Chatter}} &= 3\sin(30\pi t) + 2.5\sin(60\pi t) + 2\sin(90\pi t) \\ &\quad + 3(1 + 0.6\sin(30\pi t))\cos(600\pi t + 1.5\sin(30\pi t)) \end{aligned} \tag{20}$$

$$\begin{aligned} X_{\text{Severe−Chatter}} &= 3\sin(30\pi t) + 2.5\sin(60\pi t) + 2\sin(90\pi t) \\ &\quad + 15(1 + 0.6\sin(30\pi t))\cos(600\pi t + 1.5\sin(30\pi t)) \end{aligned} \tag{21}$$

A stable signal is simulated by summing several small-amplitude sinusoidal signals, as shown in Eq. (19). The three terms are used to represent the frequency of tooth passing and its harmonics. The weak chatter signal (Eq.(20)) is simulated by introducing a small-amplitude sinusoidal signal on the basis of another stable signal. As shown in Eq. (21), the difference between severe chatter and weak chatter lies in the magnitude of the introduced sinusoidal signal. In the numerical simulation, the spindle frequency (SF) is 15 Hz, and the chatter frequency is 300 Hz.

In this paper, the stable state is defined as the absence of chatter frequencies in the spectrum. The main distinction between weak chatter and severe chatter is that chatter frequencies in the severe chatter spectrum become the
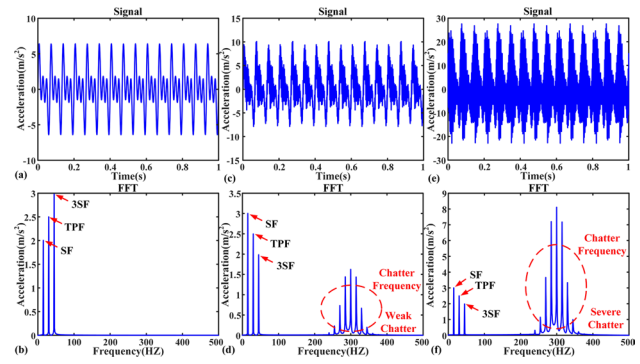

Fig. 1 Time-domain (TD) and frequency-domain (FD) diagrams of three simulation signals: **a** TD of stable signal, **b** FD of stable signal, **c** TD of weak chatter signal, **d** FD of weak chatter signal, **e** TD of severe chatter signal, and **f** FD of severe chatter signal
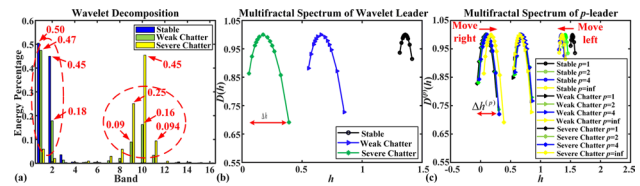

Fig. 2 Analysis results of the three feature extraction methods for simulation signals: **a** Wavelet packet method (WPM), **b** Wavelet leader multifractal method (WLMM), and **c** *p*-leader multifractal method (PLMM)

dominant peak and acceleration amplitude dramatically changes. Figure 1 shows the TD and FD analyses of the simulated signals. The FD of stable signal is the SF, tooth passing frequency (TPF), and multiplication of the SF. Although the SF, TPF, and 3SF are still the dominant peaks in the frequency spectrum when weak chatter occurs, the chatter frequency appears at this time. In severe chatter, the acceleration dramatically increases, and the dominant frequency of the spectrum becomes the chatter frequency.

The simulated signals are evaluated by the WPM, WLMM, and PLMM, as shown in Fig. 2. The frequency chosen for the numerical simulation is $f_s = 1024$ Hz, using a four-layer wavelet packet for decomposition to obtain 16 bands. The step length of frequency band is obtained from $\frac{f_s}{2 \times 16}$, then the energy information of bands 1, 2, …, 16 corresponds to the frequency ranges 0–32, 32–64, …, 480–512 Hz. Thus, the energy percentage of stable and weak chatter signals mainly focus on bands 1 and 2 (SF, TPF, and 3SF located in those bands) in Fig. 2a, and the partial energy percentage of weak chatter appear in bands 9 and 10 (chatter frequency located in these bands). Meanwhile, the energy percentage of severe chatter is

concentrated in bands 9 and 10. Therefore, it is assumed that significant chatter can be identified by the energy percentage.

The multifractal spectrum presents different spectral patterns under different p values in PLMM. The p values chosen in this study are 1, 2, 4, and inf. When $p = $ inf, PLMM becomes WLMM, as mentioned in Eq. (11). Figure 2b shows different signals with different Δh, which are the largest in severe chatter signal and the smallest in stable signal. In the p-leader multifractal spectrum (Fig. 2c), the phenomenon of $\Delta h^{(p)}$ still exists because PLMM is improved based on WLMM. Additionally, the spectral wires show a shift to the right in weak chatter and severe chatter signals and to the left in stable signal.

The simulated signals are periodic and cannot fully demonstrate the pattern recognition performance of fractal analysis methods. In the following sections, the feature extraction performance of the three methods will be analyzed with experiments.

3.2 Experimental Setup

A five-axis CNC machining center (Decklemacheo DMU-P60, shown in Fig. 3) was selected for the milling of AISI-1040. The cutting tool is a two-flute end-milling cutter with a helix angle of 30° and an approximate rake angle of 10°. Two ICP accelerometers (sensitivity of 100 mV/g) were used to collect X- and Y-direction vibration signals. The chatter frequency of the machining system is 1344 Hz [20].

3.3 TD and FD Analysis of the Experimental Tests

The acceleration signals in the X-direction of the three tests (stable signal (14,000 rpm, 0.5 μm/tooth), weak chatter

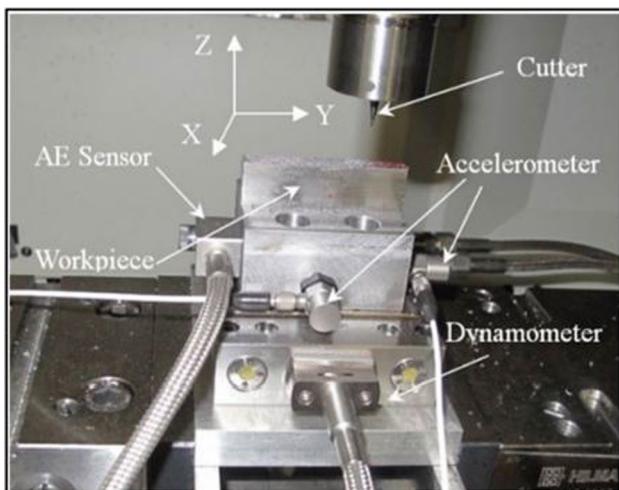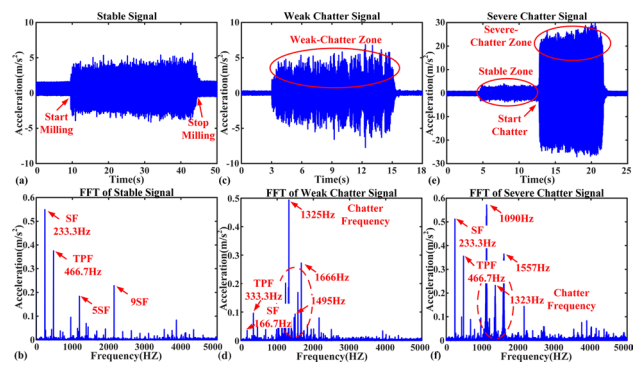**Fig. 4** Time-domain (TD) and frequency-domain (FD) diagrams of the three tests: **a** TD of stable signal, **b** FD of stable signal, **c** TD of weak chatter signal, **d** FD of weak chatter signal, **e** TD of severe chatter signal, and **f** FD of severe chatter signal

(10,000 rpm, 2 μm/tooth), and severe chatter (14,000 rpm, 1 μm/tooth)) were selected for the study, as shown in Fig. 4. In Fig. 4a, b, the cutting process lasts from 10–44 s with an acceleration amplitude of approximately 3.8 m/s². The dominant peak occurs at SF, TPF, and other peaks, which are integer multiples of SF. As shown in Fig. 4c, d, although the weak chatter test and stable test have similar acceleration values, there is a dominant peak in the FD close to the chatter frequency of 1325 Hz. In addition, the difference between peaks 1666, 1495, and 1325 Hz happens to be the SF, which indicates that the spindle rotation underwent modulation. Figure 4c, e show that the TDs of the severe chatter test and weak chatter test are significantly different, and the acceleration amplitude in the chatter zone significantly increases (close to 25 m/s²). Figure 4f shows the chatter frequency, where the difference between peaks 1557, 1323, and 1090 Hz is the SF, which is similar to weak chatter.

3.4 WPM for Chatter Detection

Figure 5 illustrates the energy percentage and WPD energy entropy for the three tests. In Fig. 5a, the energy percentage of weak chatter and severe chatter are mainly
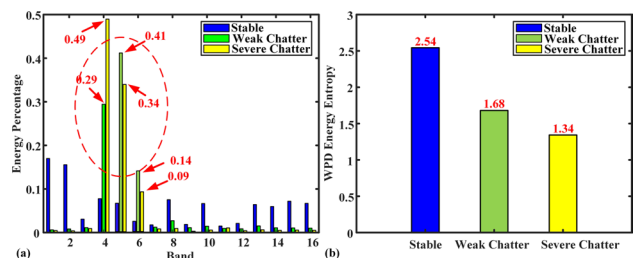

Fig. 3 Experimental setup

Fig. 5 Energy percentage and wavelet packet decomposition (WPD) energy entropy for the three tests: **a** Energy percentage and **b** WPD energy entropy

concentrated in bands 4–6 (the bands where the chatter frequency is located), which are 0.29, 0.14, and 0.41 and 0.49, 0.09, and 0.34, respectively, indicating that the energy of signal is attracted to the vicinity of the chatter frequency when chatter occurs. In Fig. 5b, the WPD energy entropy gradually decreases with the increase in signal instability, reaching the highest value of 2.54 in stable signal and the lowest value of 1.34 in severe chatter.

Therefore, the WPM can identify the processing state by analyzing the energy percentage and WPD energy entropy of the signal. However, the analysis needs to be combined with the chatter frequency, and the fluctuating value energy entropy cannot be extracted as a specific index. Hence, this method cannot accurately identify stable signals, weak chatter, and severe chatter, and the chatter recognition performance would be poor.

3.5 WLMM for Chatter Detection

The WLMM was performed for the three tests, and the results are shown in Fig. 6. The spectral width of the multifractal spectrum represents the singularity of a signal, whereas a greater singularity represents a larger spectral width. In this paper, the spectral width is denoted by Δh. As shown in Fig. 6, Δh of the stable test is smaller than that of the chatter test. In addition, $D(h_{min}) > D(h_{max})$ for the stable and weak chatter tests.

Thus, this method can accurately recognize the severe chatter by analyzing $D(h_{min})$ and $D(h_{max})$. However, it can only make a simple difference between stable and weak chatter by Δh with low precision. Evidently, the method has some advantages over the WPM in detecting severe chatter.
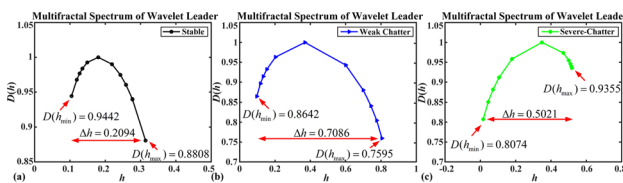
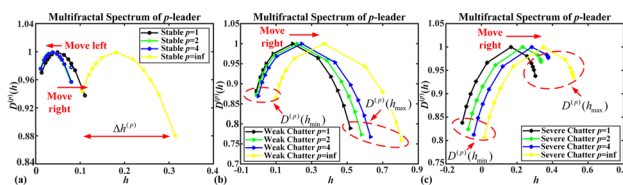**Fig. 6** Multifractal spectrum of the wavelet leader for the three tests: **a** Stable, **b** Weak chatter, and **c** Severe chatter

Fig. 7 Multifractal spectrum of the p-leader for the three tests: **a** Stable, **b** Weak chatter, and **c** Severe chatter

Table 1 Parameter indexes under different p values

Cutting conditions	Parameter indexes	$p=1$	$p=2$	$p=4$	$p=\inf$
Stable	$\Delta h^{(p)}$	0.0976	0.0681	0.0690	0.2094
	$D^{(p)}(h_{min})$	0.9708	0.9771	0.9763	0.9442
	$D^{(p)}(h_{max})$	0.9383	0.9579	0.9577	0.8808
Weak chatter	$\Delta h^{(p)}$	0.5294	0.5918	0.6314	0.7086
	$D^{(p)}(h_{min})$	0.8812	0.8727	0.8692	0.8642
	$D^{(p)}(h_{max})$	0.7890	0.7733	0.7677	0.7595
Severe chatter	$\Delta h^{(p)}$	0.4113	0.4099	0.4188	0.5022
	$D^{(p)}(h_{min})$	0.8381	0.8243	0.8125	0.8074
	$D^{(p)}(h_{max})$	0.9380	0.9683	0.9770	0.9355

3.6 PLMM for Chatter Detection

The p-spectrum of the stable test is close to a normal distribution, as presented in Fig. 7a. The p spectra first moved to the left and then to the right as p increased, which indicates a poor dependence of the stable test on p values. As shown in Figs. 7b, c, the p spectra of weak chatter and severe chatter show a significant movement toward the large value of h when the p value increases from 1 to inf, which indicates that the chatter tests have a significant dependence on the p value.

Based on the data in Fig. 7, Table 1 shows the parameter indexes of the three tests. $\Delta h^{(p)}$ of the stable test is smaller than those of the weak chatter and severe chatter test under different p values, which suggests that the chatter signals have a greater singularity. For all spectral wires, $D^{(p)}(h_{min}) > D^{(p)}(h_{max})$ for the stable and weak chatter tests, whereas $D^{(p)}(h_{min}) < D^{(p)}(h_{max})$ for the severe chatter test.

Therefore, we can correctly determine stable, weak chatter, and severe chatter by analyzing the movement patterns of spectral lines, $\Delta h^{(p)}$, $D^{(p)}(h_{min})$ and $D^{(p)}(h_{max})$ in the PLMM.

3.7 Comparison of the WPM, WLMM, and PLMM in Chatter Detection

The recognition performance criteria can be determined by the ability to accurately identify the processing state,

Table 2 Identification performance comparison of the three methods

	Stable	Weak chatter	Severe chatter	Time consumption (s)
WPM	2	1	2	5–10
WLMM	2	2	3	10–15
PLMM	3	3	3	50–70

which can be represented by 1 for normal, 2 for better, and 3 for excellent. Specifically, 1 denoted that the weak chatter state cannot be recognized, and 3 indicated that stable, weak chatter and severe chatter states can be accurately recognized. 2 indicated that the weak chatter state can be identified, but the accuracy cannot be guaranteed. For example, the WLMM cannot accurately determine whether the processing state is stable or weak chatter when Δh lies at an intermediate value. Table 2 shows the performance comparison of the three methods proposed in this paper for chatter detection. The times required for the WPM, WLMM, and PLMM calculations were approximately 5–10, 10–15, and 50–70 s, respectively, which also depends on the length of signals to some extent. Moreover, the PLMM has the best recognition performance but takes the longest time, whereas the WPM has the worst recognition performance but takes the shortest time.

4 Conclusions

In this paper, three chatter identification approaches for the milling process are presented and compared. To verify the discriminative ability of WPM, WLMM, and PLMM for different signals, a numerical simulation was first conducted to test their pattern recognition performance. Then, stable, weak chatter, and severe chatter tests were performed for the analysis, and the results confirmed that the three methods show different results for different signals. The experimental results show that the three proposed methods can distinguish different machining states. Moreover, the PLMM can effectively monitor the occurrence of weak chatter and severe chatter and presents the best recognition performance compared to WPM and WLMM. In summary, the three approaches can be widely utilized in industrial processing operations.

Author Contributions All authors read and approved the final manuscript.

Data Availability The data that support the findings of this study are available from the corresponding author upon reasonable request.

Declarations

Conflict of Interest The authors declare that they have no known competing financial interests or personal relationships that could have appeared to influence the work reported in this paper.

References

1. Altintas Y, Stepan G, Merdol D, Dombovari Z (2008) Chatter stability of milling in frequency and discrete time domain. CIRP J Manuf Sci Technol 1(1):35–44
2. Uekita M, Takaya Y (2017) Tool condition monitoring technique for deep-hole drilling of large components based on chatter identification in time–frequency domain. Measurement 103:199–207
3. Cao H, Zhang X, Chen X (2017) The concept and progress of intelligent spindles: a review. Int J Mach Tools Manuf 112:21–52
4. Lauro CH, Brandão LC, Baldo D, Reis RA, Davim JP (2014) Monitoring and processing signal applied in machining processes: a review. Measurement 58:73–86
5. Grossmann A, Kronland-Martinet R, Morlet J (1989) Reading and understanding continuous wavelet transforms. Springer, Berlin
6. Sun Y, Xiong Z (2016) An optimal weighted wavelet packet entropy method with application to real-time chatter detection. IEEE-Asme Trans Mechatron 21(4):2004–2014
7. Zhang Z, Li H, Meng G, Tu X, Cheng C (2016) Chatter detection in milling process based on the energy entropy of VMD and WPD. Int J Mach Tools Manuf 108:106–112
8. Yao YC, Chen YH, Liu CH, Shih WP (2019) Real-time chatter detection and automatic suppression for intelligent spindles based on wavelet packet energy entropy and local outlier factor algorithm. Int J Adv Manuf Technol 103(1–4):297–309
9. Hao Y, Zhu L, Yan B, Qin S, Cui D, Lu H (2022) Milling chatter detection with WPD and power entropy for Ti–6Al–4V thin-walled parts based on multi-source signals fusion. Mech Syst Signal Process 177:109225
10. Ji Y et al (2018) Early milling chatter identification by improved empirical mode decomposition and multi-indicator synthetic evaluation. J Sound Vib 433:138–159
11. Wang L, Liang M (2009) Chatter detection based on probability distribution of wavelet modulus maxima. Robot Comput-Integrated Manuf 25(6):989–998
12. Liu H, Wang X, Lu C (2015) Rolling bearing fault diagnosis based on LCD–TEO and multifractal detrended fluctuation analysis. Mech Syst Signal Process 60–61:273–288
13. Lashermes B, Jaffard S, Abry P (2005) Wavelet leader based multifractal analysis. In: Proceedings. (ICASSP '05). IEEE international conference on acoustics, speech, and signal processing
14. Du W, Tao J, Li Y, Liu C (2014) Wavelet leaders multifractal features based fault diagnosis of rotating mechanism. Mech Syst Signal Process 43(1):57–75
15. Gadhoumi K, Do D, Badilini F, Pelter MM, Hu X (2018) Wavelet leader multifractal analysis of heart rate variability in atrial fibrillation. J Electrocardiol 51(6):S83–S87
16. Pnevmatikos N, Konstandakopoulou F, Blachowski B, Papavasileiou G, Broukos P (2020) Multifractal analysis and wavelet leaders for structural damage detection of structures subjected to earthquake excitation. Soil Dyn Earthq Eng 139:106328
17. Leonarduzzi R et al (2016) P-exponent and p-leaders, Part II: multifractal analysis. Relations to detrended fluctuation analysis. Physica A: Stat Mech Appl 448:319–339
18. Leonarduzzi RF, et al (2015) p-Leader based classification of first stage intrapartum fetal HRV

19. Leonarduzzi R et al. P-leader multifractal analysis and sparse SVM for intrapartum fetal acidosis detection. In: Engineering in medicine and biology society, pp 1971–1974

20. Jing X, Zheng Z, Xu J, Wang F, Jaffery SHI, Li H (2022) Stability analysis in micro milling based on p-leader multifractal method. J Manuf Process 77:495–507

21. Zhang Z, Liu C, Liu X, Zhang J (2018) Research on the state analysis method of milling vibration using wavelet packet energy entropy. J Mech Eng 54:57–62

22. Sun Y, Cao Y, Li P (2022) Fault diagnosis for train plug door using weighted fractional wavelet packet decomposition energy entropy. Accid Anal Prev 166:106549

23. Wendt H, Roux SG, Jaffard S, Abry P (2009) Wavelet leaders and bootstrap for multifractal analysis of images. Signal Process 89(6):1100–1114

24. Wendt H, Abry P, Jaffard S (2007) Bootstrap for empirical multifractal analysis. Signal Process Mag IEEE 24(4):38–48

25. Serrano E, Figliola A (2009) Wavelet leaders: a new method to estimate the multifractal singularity spectra. Physica A: Stat Mech Appl 388(14):2793–2805

26. Jaffard S et al (2016) P-exponent and p-leaders, Part I: negative pointwise regularity. Physica A: Stat Mech Appl 448:300–318

27. Jaffard S, Abry P, Roux S (2011) Function spaces vs. scaling functions: tools for image classification. Springer, Berlin

28. Jaffard S (2006) Wavelet techniques for pointwise regularity. Ann Fac Sci Toulouse Math 1(1):3–33

29. Cao H, Lei Y, He Z (2013) Chatter identification in end milling process using wavelet packets and Hilbert-Huang transform. Int J Mach Tools Manuf 69:11–19

30. Chen Y, Li HZ, Hou L, Bu XJ, Ye SG, Chen D (2022) Chatter detection for milling using novel p-leader multifractal features. J Intell Manuf 33(1):121–135

Zehui Zheng is a prospective graduate student in mechanical engineering. He is currently pursuing his master's degree in the School of Mechanical Engineering at Tianjin University. His research focuses on milling stability and finite element simulation analysis. He has published 3 SCI and EI indexed papers. Applied for 2 invention patents.

Xiubing Jing received her Ph.D. degree in mechanical engineering from Tianjin University, Tianjin, China. She is currently an associate professor in the School of Mechanical Engineering at Tianjin University. Her areas of research interests include mechanical dynamics, surface engineering, micro/meso scale manufacturing technology. She has published over 40 peer-reviewed technical papers in international journals and conference proceedings.

Yangyang Wang is a prospective master candidate in Mechanical Engineering. He is currently pursuing a master's degree in mechanical engineering at School of Mechanical Engineering, Tianjin University. His research interests include finite element modeling and thermal error analysis of machine tools.

Xiaofei Song received her Ph.D. degree in mechanical engineering from Tianjin University, Tianjin, China. She is currently an associate professor in the School of Mechanical Engineering at Tianjin University. Her research focuses on structure-property-process relations of biomaterials, advanced machining of biological tissues in medical surgery including ultrasonic cutting of hard tissue and waterjet ablation of soft tissue. She is a committee member of Holistic Integrative Medicine Society (HIM) of Tianjin and a senior member of the Chinese Mechanical Engineering Society (CMES).

Dr Huaizhong Li obtained a PhD degree from the National University of Singapore. He is currently a Senior Lecturer at the School of Engineering and Built Environment, Griffith University, Australia. He is a Fellow of International Academy of Engineering and Technology (AET), Fellow of the Higher Education Academy (FHEA), and Fellow of the Griffith Learning and Teaching Academy. His research interests include advanced manufacturing technologies, micromachining, machine dynamics, vibration monitoring and control, and mechatronics.